Contents lists available at ScienceDirect

Catalysis Communications

Short Communication

Decomposition of high-level ozone under high humidity over Mn–Fe catalyst: The influence of iron precursors

Zhihua Lian, Jinzhu Ma, Hong He *

State Key Joint Laboratory of Environment Simulation and Pollution Control, Research Center for Eco-Environmental Sciences, Chinese Academy of Sciences, Beijing 100085, PR China

ABSTRACT

Manganese–iron mixed oxide, an efficient and stable catalyst, has been successfully used in the decomposition of ozone. The influence of different iron precursors on the catalytic decomposition activity of high-level ozone under high-humidity over manganese–iron catalysts prepared using a hydrothermal approach was studied. The catalytic performance over $MnFe_{0.5}O_x–Fe(NO_3)_3$ was much better than that of $MnFe_{0.5}O_x–FeSO_4$ and $MnFe_{0.5}O_x–FeCl_3$. From the results of characterization by N_2 physical adsorption, XRD, XPS and SEM, it was concluded that the largest specific surface area, the lowest crystallinity, the most evenly distributed particle size and the most surface-active Mn^{2+} and Mn^{3+} led to the best catalytic activity for the $MnFe_{0.5}O_x–Fe(NO_3)_3$ catalyst.

© 2014 Elsevier B.V. All rights reserved.

1. Introduction

As a strong oxidant, ozone has been widely used in drinking water and wastewater treatment for disinfection and oxidation (e.g., taste and odor control, decolorization, and elimination of micropollutants) [1–5]. The resulting tail gas still contains some amount of ozone, which should be removed before discharge. Some modern indoor devices such as photocopiers, laser printers, and ozone disinfection machines also encounter the problem of ozone emission. Tropospheric ozone is a common pollutant that causes health problems to human beings including reduced lung function, increased frequency of respiratory symptoms, and development of asthma [6,7]. Because of its toxicity, the Occupational Safety and Health Administration (OSHA, the United States of America) has set the maximum human allowable exposure to ozone for an eight-hour period at 0.10 ppm [8]. Chinese 'indoor air quality standards' (GB/T 18883-2002) requires that indoor ozone concentration should not exceed 0.16 mg/m^3 (0.07 ppm) [9]. Thus, it is urgently necessary to develop effective methods to eliminate ozone in order to protect human health from the increasing ozone exposure in our environment.

Various methods such as dilution, liquid absorption, thermal decomposition and catalytic decomposition have been reported to control ozone emission [10–13]. Among them, catalytic decomposition is the most widely used method, due to its advantages of mild reaction conditions, high efficiency and low cost. Numerous catalysts have been investigated, including transition metal oxides [14–21], activated carbon [22,23] and noble metals [24–26]. Among these catalysts, manganese oxides (MnO_x) usually show good catalytic performance in ozone decomposition. However, the catalytic activity tends to decrease with coexisting water vapor and operation time [20,21].

In this study, the modification of MnO_x by adding Fe and the influence of different iron precursors on the catalytic decomposition activity of high-level ozone under high humidity over manganese–iron oxides catalysts were investigated. The $MnFe_{0.5}O_x–Fe(NO_3)_3$ catalyst exhibited the best catalytic activity and stability, which was related to it possessing the largest specific surface area, the lowest crystallinity, the most surface-active Mn^{2+} and Mn^{3+} and the most evenly distributed particle size.

2. Experimental

2.1. Catalyst synthesis and activity test

The Mn–Fe catalysts were synthesized by hydrothermally treating a suspension containing $MnSO_4 \cdot H_2O$, $KMnO_4$ and the desired amount of Fe precursors in a Teflon-lined autoclave at 100 °C for 24 h. The resulting black slurry was centrifuged, washed by deionized water and dried at 100 °C overnight, followed by calcination at 350 °C in air for 3 h for characterization and evaluation of catalytic performance. MnO_x was also prepared by the same process. Mn–Fe catalysts with different ratios of Fe/Mn were prepared using $Fe(NO_3)_3$ as Fe precursor. The Fe precursors of $MnFe_{0.5}O_x–FeCl_3$ and $MnFe_{0.5}O_x–FeSO_4$ catalysts were $FeCl_3$ and $FeSO_4$, respectively.

Ozone decomposition was studied in a flow reactor at ambient temperature (25 °C). The reaction conditions were controlled as follows:

---

ozone concentration 21.43 g/m^3 (10,000 ppm), air balance, gas flow 40 mL/min, catalyst 0.2 g, 40% or 90% relative humidity. Ozone concentration was recorded with an ozone analyzer (2B Technology, US). Ozone conversion was calculated as follows:

$$O_3 \text{ conversion} = \frac{C_{in} - C_{out}}{C_{in}}.$$

2.2. Characterization of catalysts

The surface area and pore characterization of the catalysts were obtained from N$_2$ adsorption/desorption analysis at −196 °C using a Quantachrome Quadrasorb SI-MP. Prior to the N$_2$ physisorption, the catalysts were degassed at 300 °C for 5 h. Surface areas were determined using the BET equation in the 0.05–0.35 partial pressure range. Pore volumes and average pore diameters were determined by the Barrett–Joyner–Halenda (BJH) method from the desorption branches of the isotherms.

Powder X-ray diffraction (XRD) measurements of the catalysts were carried out on a computerized PANalytical X'Pert Pro diffractometer with Cu Kα (λ = 0.15406 nm) radiation. The data of 2θ from 10 to 90° were collected at 8°/min with step size of 0.07°.

X-ray photoelectron spectroscopy (XPS) results of the catalysts were recorded on a scanning X-ray microprobe (Axis Ultra, Kratos Analytical Ltd.) using Al Kα radiation (1486.7 eV).

The surface morphology of the samples was studied using a field-emission scanning electron microscope (FESEM, Hitachi, SU-8020). The accelerating voltage was 3.0 kV.

3. Results and discussion

3.1. Catalytic performance

Fig. 1 shows ozone conversion as a function of time over Mn–Fe catalysts. The initial catalytic activity over all the catalysts was 100% at 25 °C. Ozone conversion over the MnO$_x$ catalyst decreased quickly and only 40% conversion was obtained after 30 min under 90% relative humidity. The addition of Fe enhanced catalytic activity remarkably. With the increase of Fe content, catalytic activity over Mn–Fe catalysts increased. MnFe$_{0.5}$O$_x$ exhibited the best catalytic performance and maintained as high as 90% ozone conversion after an 8 h test. Any further increase in Fe content resulted in a decline in activity.

Different precursors could affect structural properties of catalysts such as dispersion, crystallinity and morphology [27,28] and then influence catalytic performance. Thus the influence of Fe precursors on
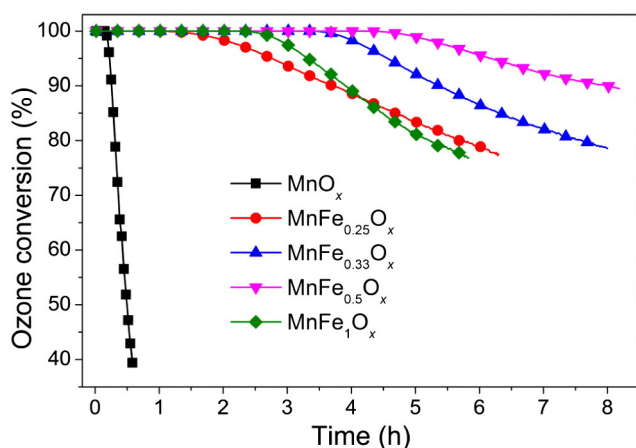

Fig. 1. Ozone conversion as a function of time over Mn–Fe catalysts (ozone initial concentration 21.43 g/m^3, temperature 25 °C, weight space velocity 12 L/(g·h), RH >90%).
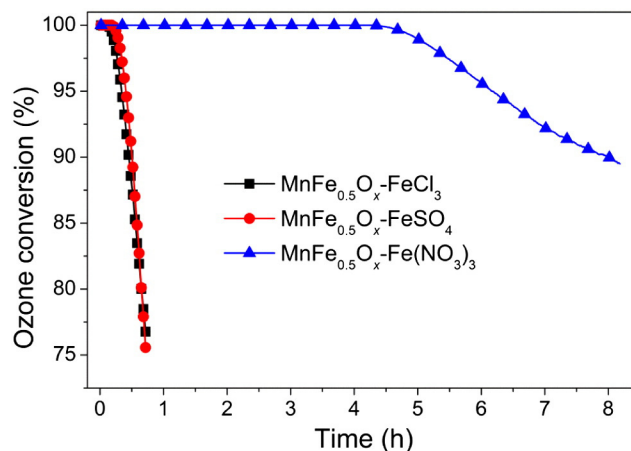

Fig. 2. Ozone conversion as a function of time over MnFe$_{0.5}$O$_x$ catalysts of different precursors (ozone initial concentration 21.43 g/m^3, temperature 25 °C, weight space velocity 12 L/(g·h), RH >90%).

catalytic ozone conversion was investigated and the results are shown in Fig. 2. MnFe$_{0.5}$O$_x$–FeSO$_4$ and MnFe$_{0.5}$O$_x$–FeCl$_3$ catalysts exhibited similar catalytic performance. Ozone conversion decreased quickly to 80% after a 40 min test. However, the MnFe$_{0.5}$O$_x$–Fe(NO$_3$)$_3$ catalyst showed the best catalytic performance and still maintained 90% ozone conversion after an 8 h test. In the following sections, we will investigate the influence of precursors on structure, morphology and surface properties of MnFe$_{0.5}$O$_x$ catalysts using various characterization methods.

3.2. Catalyst characterization

N$_2$ adsorption–desorption isotherms and the pore size distributions of MnFe$_{0.5}$O$_x$ and MnO$_x$ catalysts are shown in Fig. S1 and Fig. S2. The MnFe$_{0.5}$O$_x$–Fe(NO$_3$)$_3$ catalyst showed type IV isotherms, which are typical for mesoporous materials (2–50 nm pore diameter). The addition of Fe to MnO$_x$ decreased the pore diameter.

Calculated from the isotherms, the surface area and pore characterization of MnFe$_{0.5}$O$_x$ and MnO$_x$ catalysts are shown in Table 1. MnO$_x$ exhibited the smallest specific surface area and the largest average pore diameter. The addition of Fe led to the increase of surface area and the decrease of pore diameter. Furthermore, the specific surface area and pore volume of the MnFe$_{0.5}$O$_x$–Fe(NO$_3$)$_3$ catalyst were clearly larger than that of MnFe$_{0.5}$O$_x$–FeSO$_4$ and MnFe$_{0.5}$O$_x$–FeCl$_3$ catalysts. The large specific surface area and pore volume of the MnFe$_{0.5}$O$_x$–Fe(NO$_3$)$_3$ catalyst are beneficial for ozone decomposition, as shown in Fig. 2.

XRD patterns of MnFe$_{0.5}$O$_x$ and MnO$_x$ catalysts are shown in Fig. 3. The MnO$_x$ catalyst displayed well-defined diffraction peaks attributed to α-MnO$_2$ (JCPDS 44-0141). The diffraction peaks of MnFe$_{0.5}$O$_x$–FeSO$_4$ and MnFe$_{0.5}$O$_x$–FeCl$_3$ catalysts were also consistent with the α-MnO$_2$ structure, but the intensity was notably decreased compared with that of MnO$_x$ catalyst, indicating that the addition of Fe led to a decrease in MnO$_2$ crystallinity. The diffraction line of the MnFe$_{0.5}$O$_x$–Fe(NO$_3$)$_3$ catalyst around 37.5° was shifted slightly to the lower angle region (from 37.49° to 36.86°) compared to that of MnO$_x$. This may be due to the existence of a Mn–Fe solid solution oxide.

Table 1
The surface area and pore characterization of MnFe$_{0.5}$O$_x$ and MnO$_x$ catalysts.

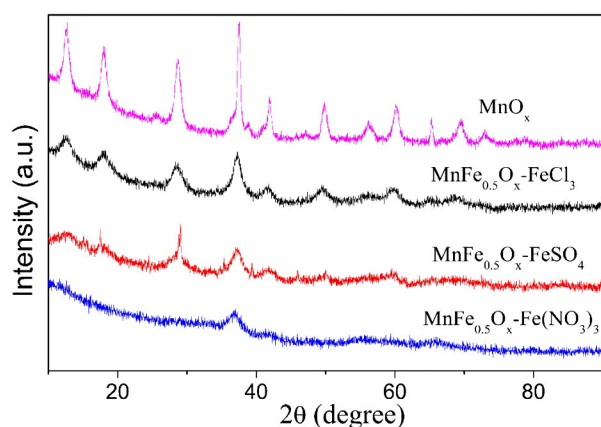| Catalysts	Specific surface area (m^2/g)	Pore volume (cm^3/g)	Pore diameter (nm)
MnO$_x$	71.7	0.612	34.2
MnFe$_{0.5}$O$_x$–FeCl$_3$	172	0.285	6.60
MnFe$_{0.5}$O$_x$–FeSO$_4$	168	0.238	4.90
MnFe$_{0.5}$O$_x$–Fe(NO$_3$)$_3$	262	0.573	5.63

Fig. 3. XRD patterns of $MnFe_{0.5}O_x$ and MnO_x catalysts.

Table 2
Surface and bulk atomic concentration on $MnFe_{0.5}O_x$ catalysts.

Catalysts	Surface atomic concentration (%)					Fe/Mn (surface)	Fe/Mn[a] (bulk)
	Mn	Fe	O	Cl	S		
$MnFe_{0.5}O_x$–$FeCl_3$	28.07	9.31	60.62	0.79	1.22	0.33	0.23
$MnFe_{0.5}O_x$–$FeSO_4$	25.24	10.99	61.12	0.74	1.91	0.44	0.37
$MnFe_{0.5}O_x$–$Fe(NO_3)_3$	30.04	8.25	59.47	0.79	1.44	0.28	0.24

[a] Derived from ICP-OES results.

However, compared to other catalysts, the diffraction peaks of $MnFe_{0.5}O_x$–$Fe(NO_3)_3$ weakened significantly, indicating that the catalyst was nearly amorphous. Furthermore, no extra peaks attributed to iron species were detected, suggesting that iron species were highly dispersed or were amorphous in these samples. The low crystallinity over the $MnFe_{0.5}O_x$–$Fe(NO_3)_3$ catalyst indicated more defects and possibly enhanced the surface area, which could favor the ozone decomposition.

XPS can be used to investigate the surface composition and surface elemental valence on $MnFe_{0.5}O_x$ catalysts of different precursors. The surface atomic concentrations of Mn, Fe, and O on $MnFe_{0.5}O_x$ catalysts are shown in Table 2. Not only the surface Fe/Mn molar ratios on the three catalysts but also the Fe/Mn molar ratios in the bulk derived from ICP-OES were lower than the molar ratio of the raw materials. This indicated that Fe was not fully used in the process of hydrothermal synthesis. The $MnFe_{0.5}O_x$–$Fe(NO_3)_3$ catalyst showed a higher surface Mn concentration and lower surface Fe/Mn molar ratio than other catalysts. There was almost no difference in the contents of S and Cl in the $MnFe_{0.5}O_x$ catalysts prepared from different precursors.

XPS of Mn 2p, Fe 2p and O 1s is shown in Fig. S3. $MnFe_{0.5}O_x$ catalysts of three different precursors including $FeCl_3$, $FeSO_4$, and $Fe(NO_3)_3$ showed similar Fe 2p spectra. The XPS of O 1s was deconvoluted into three peaks, including the lattice oxygen (denoted as O_β), the surface adsorbed oxygen (denoted as O_α) and chemisorbed water (denoted as O_α'). The XPS of Mn 2p was also deconvoluted into three peaks, and Table 3 presents the surface Mn valence distribution on the $MnFe_{0.5}O_x$ catalysts prepared from different precursors. Surface Mn on $MnFe_{0.5}O_x$–$FeSO_4$ and $MnFe_{0.5}O_x$–$FeCl_3$ catalysts existed mainly in the form of Mn^{4+}. However, the most abundant Mn^{2+} and Mn^{3+} existed on the surface of the

$MnFe_{0.5}O_x$–$Fe(NO_3)_3$ catalyst, which could be the reason for its superior catalytic performance, as discussed below.

Catalyst morphology was investigated by FESEM and the results are shown in Fig. 4. The MnO_x catalyst showed a nanowire structure. The addition of Fe to MnO_x altered the morphology significantly. Besides, the morphologies of $MnFe_{0.5}O_x$ catalysts were influenced by the iron precursors. $MnFe_{0.5}O_x$–$FeSO_4$ and $MnFe_{0.5}O_x$–$FeCl_3$ catalysts exhibited irregular shape and non-uniform particle size distribution, while the $MnFe_{0.5}O_x$–$Fe(NO_3)_3$ catalyst exhibited more regular spherical particles, smaller particle size and more uniform particle size distribution.

The $MnFe_{0.5}O_x$ catalysts showed different specific surface areas, crystallinity, morphology and surface Mn valence distribution with the different iron precursors. In the hydrothermal process, slight differences in pH in the solution could lead to distinct morphology and structure variations [29,30]. The experimental temperature, precursor, surfactants and pH control the crystallization of metal oxides with controlled sizes and shapes [31]. Manganese precursors could affect the crystal phase, pore structure and Mn dispersion and then influence oxidative activity [32]. In light of these previous reports, we suggested that the different iron precursors including $FeCl_3$, $FeSO_4$ and $Fe(NO_3)_3$ could lead to different pH and ionic strength in the solution and then affect the hydrolysis rate and nucleation rate of Mn and Fe. Finally, it could result in different structure, morphology, surface composition and surface elemental valence for the catalysts. The MnO_x catalyst showed different structural properties from the Mn–Fe oxide catalysts. The doped metal oxide influenced the structure and morphology of the catalyst [33]. The addition of Fe to MnO_x affected the nucleation process and then decreased the crystallinity of the catalysts. The highest specific surface area for $MnFe_{0.5}O_x$–$Fe(NO_3)_3$ may be due to it having the lowest crystallinity. Therefore, the $MnFe_{0.5}O_x$ catalyst derived from $Fe(NO_3)_3$ showed the highest specific surface area, the lowest crystallinity, the most evenly distributed particle size and the most surface-active Mn^{2+} and Mn^{3+}.

3.3. Stability test

Water vapor has a severe influence on catalytic performance in ozone decomposition. The stability of the $MnFe_{0.5}O_x$–$Fe(NO_3)_3$ catalyst was investigated under low humidity and the result is shown in Fig. 5. The ozone conversion was still maintained at 100% after a 66 h test under 40% relative humidity (RH). The catalytic activity and stability under 90% RH were lower than for 40% RH, which could be due to the formation of a liquid film from accumulation of water molecules, preventing ozone from contacting surface active sites and thus decreasing catalytic activity [34]. The $MnFe_{0.5}O_x$–$Fe(NO_3)_3$ catalyst exhibited excellent catalytic stability and is promising for practical application.

3.4. Reaction mechanism

According to the literature [16,35], ozone decomposition follows the scheme:

$$O_3 + \left[M^{n+}\right] \rightarrow O_2 + O^- \left[M^{n+1}\right] \tag{1}$$

$$O_3 + O^- \left[M^{n+1}\right] \rightarrow 2O_2 + \left[M^{n+}\right]. \tag{2}$$

Table 3
XPS results of surface Mn species on $MnFe_{0.5}O_x$ catalysts surface.

Catalysts	$Mn^{2+} / (Mn^{2+} + Mn^{3+} + Mn^{4+})$ (%)	$Mn^{3+} / (Mn^{2+} + Mn^{3+} + Mn^{4+})$ (%)	$Mn^{4+} / (Mn^{2+} + Mn^{3+} + Mn^{4+})$ (%)
$MnFe_{0.5}O_x$–$FeCl_3$	9.17	25.52	65.31
$MnFe_{0.5}O_x$–$FeSO_4$	10.50	29.25	60.25
$MnFe_{0.5}O_x$–$Fe(NO_3)_3$	16.37	37.66	45.97
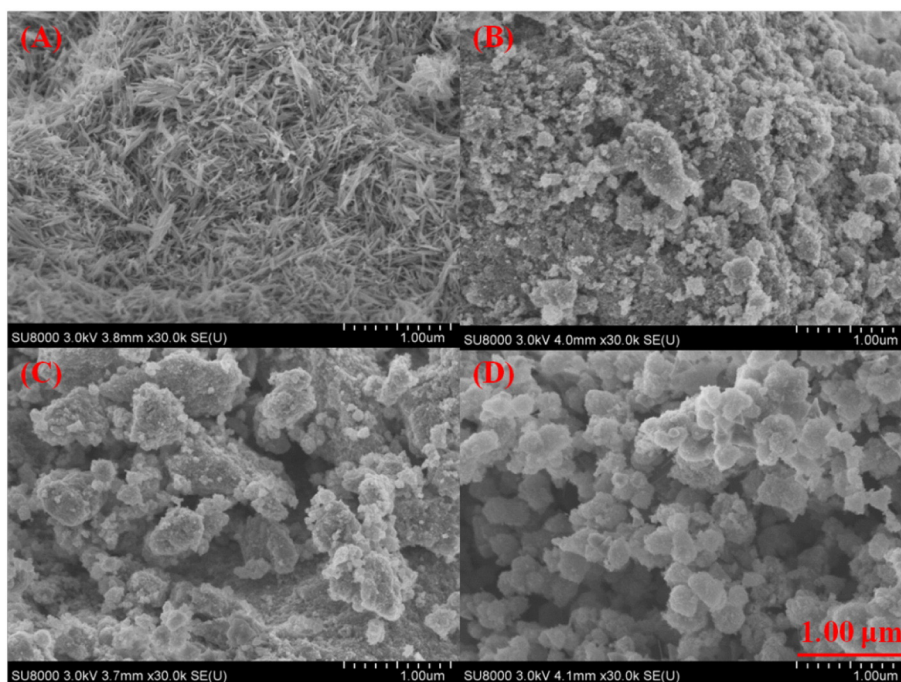
Fig. 4. FESEM images of MnO$_x$ catalyst (A), MnFe$_{0.5}$O$_x$–FeCl$_3$ catalyst (B), MnFe$_{0.5}$O$_x$–FeSO$_4$ catalyst (C), MnFe$_{0.5}$O$_x$–Fe(NO$_3$)$_3$ catalyst (D).

Transition metal oxides with several oxidation states could potentially show good catalytic performance in ozone decomposition. In the case of Mn–Fe mixed oxide catalysts, we have redox couples including Mn^{2+}–Mn^{3+}–Mn^{4+} and Fe^{2+}–Fe^{3+}. These couples could be represented by the following model for the reaction mechanism:

$$O_3 + \left[Mn^{3+}\right] \rightarrow O_2 + O^- \left[Mn^{4+}\right] \tag{3}$$

$$O_3 + O^- \left[Mn^{4+}\right] \rightarrow 2O_2 + \left[Mn^{3+}\right] \tag{4}$$

$$O_3 + \left[Mn^{2+}\right] \rightarrow O_2 + O^- \left[Mn^{3+}\right] \tag{5}$$

$$O_3 + O^- \left[Mn^{3+}\right] \rightarrow 2O_2 + \left[Mn^{2+}\right] \tag{6}$$

$$O_3 + \left[Mn^{2+}\right] \rightarrow O_2 + O^{2-} \left[Mn^{4+}\right] \tag{7}$$

$$O_3 + O^{2-} \left[Mn^{4+}\right] \rightarrow 2O_2 + \left[Mn^{2+}\right] \tag{8}$$

$$O_3 + \left[Fe^{2+}\right] \rightarrow O_2 + O^- \left[Fe^{3+}\right] \tag{9}$$

$$O_3 + O^- \left[Fe^{3+}\right] \rightarrow 2O_2 + \left[Fe^{2+}\right]. \tag{10}$$

There are two redox couples, Mn^{2+}–Mn^{3+}–Mn^{4+} and Fe^{2+}–Fe^{3+}, in Mn–Fe mixed oxides, while only Mn^{2+}–Mn^{3+}–Mn^{4+} is present in the MnO$_x$ catalyst. Thus Mn–Fe oxide catalysts showed higher catalytic activity than the MnO$_x$ catalyst. Abundant Mn^{2+} and Mn^{3+} existed on the surface of the MnFe$_{0.5}$O$_x$–Fe(NO$_3$)$_3$ catalyst (Table 3), which could favor the redox process. Therefore, the MnFe$_{0.5}$O$_x$–Fe(NO$_3$)$_3$ catalyst showed better catalytic performance than MnFe$_{0.5}$O$_x$–FeCl$_3$ and MnFe$_{0.5}$O$_x$–FeSO$_4$ catalysts, in which surface Mn mainly existed in the form of Mn^{4+}.

4. Conclusions

Mn–Fe mixed oxide catalysts prepared by a hydrothermal method showed higher catalytic ozone decomposition activity than MnO$_x$ catalyst. Among catalysts with different Fe/Mn ratios, MnFe$_{0.5}$O$_x$ exhibited the best catalytic performance. MnFe$_{0.5}$O$_x$ using Fe(NO$_3$)$_3$ as Fe precursor displayed higher ozone conversion and better stability than catalysts using FeCl$_3$ or FeSO$_4$ as Fe precursor. The ozone conversion over the MnFe$_{0.5}$O$_x$–Fe(NO$_3$)$_3$ catalyst was still maintained at 100% after a 66 h test under the reaction condition of 21.43 g/m^3 ozone initial concentration, 25 °C, 12 L/(g·h) SV and 40% relative humidity. The catalyst holds great promise for industrial application. The largest specific surface area, the lowest crystallinity, the most evenly distributed particle size and the most surface-active Mn^{2+} and Mn^{3+} were all responsible for the best catalytic activity for the MnFe$_{0.5}$O$_x$–Fe(NO$_3$)$_3$ catalyst.
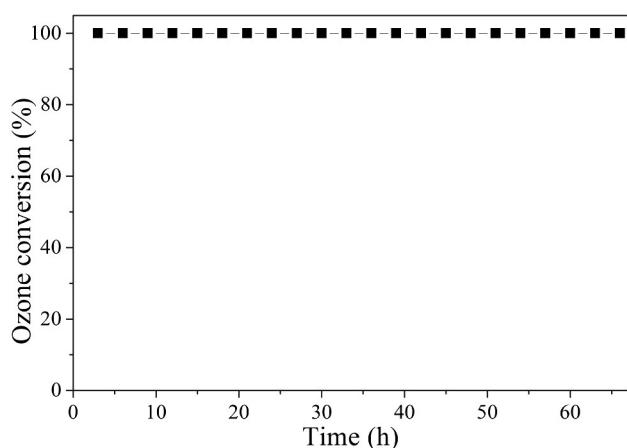

Fig. 5. Stability test result of MnFe$_{0.5}$O$_x$–Fe(NO$_3$)$_3$ catalyst (ozone initial concentration 21.43 g/m^3, temperature 25 °C, weight space velocity 12 L/(g·h),RH = 40%).

Acknowledgments

Appendix A. Supplementary data

Supplementary data to this article can be found online at http://dx.doi.org/10.1016/j.catcom.2014.10.005 These data include MOL files and InChiKeys of the most important compounds described in this article.

References

[1] V. Yargeau, C. Leclair, Ozone Sci. Eng. 30 (2008) 175–188.
[2] K. Ikehata, N. Jodeiri Naghashkar, M. Gamal El-Din, Ozone Sci. Eng. 28 (2006) 353–414.
[3] K. Ikehata, M. Gamal El-Din, Ozone Sci. Eng. 27 (2005) 173–202.
[4] K. Ikehata, M. Gamal El-Din, Ozone Sci. Eng. 27 (2005) 83–114.
[5] T.E. Agustina, H.M. Ang, V.K. Vareek, J. Photochem. Photobiol. C 6 (2005) 264–273.
[6] U. Roland, F. Holzer, E.D. Kopinke, Appl. Catal. B Environ. 58 (2005) 217–226.
[7] C.J. Weschler, Environ. Health Perspect. 114 (2006) 1489–1496.
[8] C. Heisig, W.M. Zhang, S.T. Oyama, Appl. Catal. B Environ. 14 (1997) 117–129.
[9] Q. Yu, H. Pan, M. Zhao, Z. Liu, J. Wang, Y. Chen, M. Gong, J. Hazard. Mater. 172 (2009) 631–634.
[10] R.G. Rice, A. Netzer, Ann. Arbor. Sci. Publ. 1 (1982) 341–378.
[11] T.L. Rakitskaya, E.K. Vasileva, A.Y. Bandun, V.Y. Paina, Kinet. Katal. 35 (1994) 90–92.
[12] S. Stephens, M.J. Rossi, D.M. Golden, Int. J. Chem. Kinet. 18 (1986) 1133–1149.
[13] D. Helmig, Atmos. Environ. 31 (1997) 3635–3651.
[14] B. Dhandapani, S.T. Oyama, Appl. Catal. B Environ. 11 (1997) 129–166.
[15] D. Mehandjiev, A. Naidenov, Ozone Sci. Eng. 14 (1992) 277–282.
[16] I. Spasova, P. Nikolov, D. Mehandjiev, Ozone Sci. Eng. 29 (2007) 41–45.
[17] M. Muruganandham, J.J. Wu, Catal. Commun. 8 (2007) 668–672.
[18] Z.Z. Xu, Z.L. Chen, C. Joll, Y. Ben, J.M. Shen, H. Tao, Catal. Commun. 10 (2009) 1221–1225.
[19] H. Pan, L. Zhou, Y. Zhu, N. Peng, M. Gong, Y. Chen, Chin. J. Catal. 32 (2011) 1040–1045.
[20] M. Wang, P. Zhang, J. Li, C. Jiang, Chin. J. Catal. 35 (2014) 335–341.
[21] C. Jiang, P. Zhang, B. Zhang, J. Li, M. Wang, Ozone Sci. Eng. 35 (2013) 308–315.
[22] C. Subrahmanyam, D.A. Bulushev, L. Kiwi-Minsker, Appl. Catal. B Environ. 61 (2005) 98–106.
[23] T.L. Rakitskaya, A.Y. Bandurko, A.A. Ennan, V.Y. Paina, A.S. Rakitskiy, Microporous Mesoporous Mater. 43 (2001) 153–160.
[24] B. Zhang, P. Zhang, R. Shi, H. Wang, Chin. J. Catal. 30 (2009) 235–241.
[25] A. Naydenov, P. Konova, P. Nikolov, F. Klingstedt, N. Kumar, D. Kovacheva, P. Stefanov, R. Stoyanova, D. Mehandjiev, Catal. Today 137 (2008) 471–474.
[26] C. Ren, L. Zhou, H. Shang, Y. Chen, Chin. J. Catal. 35 (2014) 1–9.
[27] K.J. Chao, L.H. Lin, M.H. Yang, Catal. Lett. 38 (1996) 279–282.
[28] F. Kapteijn, A.D.V. Langeveld, J.A. Moulijn, M. Vandriel, A. Andreini, M.A. Vuurman, A.M. Turek, J.M. Jehng, I.E. Wachs, J. Catal. 150 (1994) 94–104.
[29] S. Baruah, J. Dutta, Sci. Technol. Adv. Mater. 10 (2009) 1–18.
[30] M.S. Whittingham, Curr. Opin. Solid State Mater. 1 (1996) 227–232.
[31] K. Namratha, K. Byrappa, Prog. Cryst. Growth Charact. 58 (2012) 14–42.
[32] H. Pérez, P. Navarro, J.J. Delgado, M. Montes, Appl. Catal. A Gen. 400 (2011) 238–248.
[33] I. Andjelkovic, D. Stankovic, J. Nesic, J. Krstic, P. Vulic, D. Manojlovic, G. Roglic, Ind. Eng. Chem. Res. 53 (2014) 10841–10848.
[34] H. Yin, J. Xie, Q. Yang, C. Yin, Y. Wang, F. Feng, Chem. Res. Appl. 15 (2003) 1–5.
[35] D. Mehandjiev, A. Naydenov, G. Ivanov, Appl. Catal. A Gen. 206 (2001) 13–18.